Nano Research

ISSN 1998-0124 CN 11-5974/O4
https://doi.org/10.1007/s12274-021-3575-9

Research Article

Towards intrinsically pure graphene grown on copper

Xiaozhi Xu[1,2,§] (✉), Ruixi Qiao[3,4,§], Zhihua Liang[1,2], Zhihong Zhang[3,4], Ran Wang[1,2], Fankai Zeng[1,2], Guoliang Cui[1,2], Xiaowen Zhang[1,2], Dingxin Zou[5], Yi Guo[3], Can Liu[3], Ying Fu[6], Xu Zhou[1,2], Muhong Wu[4], Zhujun Wang[7], Yue Zhao[5], Enke Wang[1,2], Zhilie Tang[1,2], Dapeng Yu[5], and Kaihui Liu[3,4] (✉)

[1] *Guangdong Provincial Key Laboratory of Quantum Engineering and Quantum Materials, School of Physics and Telecommunication Engineering, South China Normal University, Guangzhou 510006, China*
[2] *Guangdong-Hong Kong Joint Laboratory of Quantum Matter, South China Normal University, Guangzhou 510006, China*
[3] *State Key Laboratory for Mesoscopic Physics, Frontiers Science Center for Nano-optoelectronics, School of Physics, Peking University, Beijing 100871, China*
[4] *International Centre for Quantum Materials, Collaborative Innovation Centre of Quantum Matter, Peking University, Beijing 100871, China*
[5] *Shenzhen Institute for Quantum Science and Engineering, and Department of Physics, Southern University of Science and Technology, Shenzhen 518055, China*
[6] *Songshan Lake Materials Laboratory, Institute of Physics, Chinese Academy of Sciences, Guangdong 523808, China*
[7] *School of Physical Science and Technology, Shanghai Tech University, Shanghai 200031, China*
[§] *Xiaozhi Xu and Ruixi Qiao contributed equally to this work.*

© Tsinghua University Press and Springer-Verlag GmbH Germany, part of Springer Nature 2021
Received: 15 February 2021 / **Revised:** 2 May 2021 / **Accepted:** 5 May 2021

ABSTRACT

The state-of-the-art semiconductor industry is built on the successful production of silicon ingot with extreme purity as high as 99.999999999%, or the so-called "eleven nines". The coming high-end applications of graphene in electronics and optoelectronics will inevitably need defect-free pure graphene as well. Due to its two-dimensional (2D) characteristics, graphene restricts all the defects on its surface and has the opportunity to eliminate all kinds of defects, i.e., line defects at grain boundaries and point or dot defects in grains, and produce intrinsically pure graphene. In the past decade, epitaxy growth has been adopted to grow graphene by seamlessly stitching of aligned grains and the line defects at grain boundaries were eliminated finally. However, as for the equally common dot and point defects in graphene grain, there are rare ways to detect or reduce them with high throughput and efficiency. Here, we report a methodology to realize the production of ultrapure graphene grown on copper by eliminating both the dot and point defects in graphene grains. The dot defects, proved to be caused by the silica particles shedding from quartz tube during the high-temperature growth, were excluded by a designed heat-resisting box to prevent the deposition of particles on the copper surface. The point defects were optically visualized by a mild-oxidation-assisted method and further reduced by etching-regrowth process to an ultralow level of less than 1/1,000 μm^2. Our work points out an avenue for the production of intrinsically pure graphene and thus lays the foundation for the large-scale graphene applications at the integrated-circuit level.

KEYWORDS

pure graphene, point defect, mild-oxidation, copper

1 Introduction

The purity of any functional material is essential to determine its ultimate performance in high-end applications, e.g. the cornerstone of the semiconductor industry is the mature production of ultrahigh-purity single crystals. Although the second-generation semiconductors of GaAs, InP and InSb, third-generation semiconductors of GaN, SiC, ZnO and diamond have more superior properties [1–4], they still cannot shake the position of silicon in the semiconductor industry so far. The main reason for the success of silicon lies in the fact that one can prepare extreme high-quality single-crystal silicon with purity up to "eleven nines". Graphene, due to its novel physical properties and superior device performance in ultra-high-frequency electronics and ultrafast optoelectronics, has been proved as a promising candidate for the next-generation electronic material [5–9]. Surely, the production of ultrahigh-purity graphene is the prerequisite to realize all these expecting applications.

Unlike bulk silicon whose defects are embedded in the materials, two-dimensional (2D) graphene restricts all the defects on its surface. This special feature offers a unique opportunity to detect and eliminate all the defects and produce intrinsically pure graphene, which is impossible for bulk materials. To reach this target, there are three basic issues that need to be addressed: (i) to visualize the defects with high throughput; (ii) to figure out the origins of these defects; (iii) to find a solution to eliminate these defects. At present, chemical vapour deposition (CVD) method stands out as the prevailing method to produce large-scale high-quality graphene films [10–25]. Generally, for these CVD graphene films, there are two kinds of defects: (i) line defects at the grain boundaries; (ii) nanometre-scale dot defects and atomic-scale point defects in grains. In the past decade,

Address correspondence to Kaihui Liu, khliu@pku.edu.cn; Xiaozhi Xu, xiaozhixu@scnu.edu.cn

line defects have been solved by epitaxial growth on single-crystal metal foils or single-nucleus growth [14–25]. Therefore, to obtain intrinsically pure graphene, the final mission is to eliminate the dot and point defects in graphene.

In this work, we proposed a method to synthesize intrinsically pure monolayer graphene grown on copper (Cu). Firstly, a mild-oxidation-assisted detecting technique was developed to visualize the defects in graphene, including nanometre-scale dot defects and atomic-scale point defects, by forming the visible cuprous oxide (Cu_2O) underlying the graphene defects. Then, dot defects in graphene were found to be caused by silica particles released from quartz tube at high temperature and can be eliminated by a specially designed heat-resisting box. The point defects, although are introduced by the uncontrollable thermodynamic fluctuation during growth, can be cured by a hydrogen (H_2) etching and regrowth approach. With these techniques, the dot and point defects density can be reduced to an extremely low level of less than 1/1,000 μm^2. Our work opens up a new direction for the synthesis of intrinsically pure graphene films and lays foundation for the high-end applications of graphene especially in integrated circuits.

2 Experimental

2.1 Growth of graphene

Graphene samples were grown by CVD method. Cu foils (25 μm thick, 99.8%, Alfa Aesar) were either placed in a heat-resisting box in advance or directly loaded into a CVD furnace (Hefei Kejing Company OTF1250). The system was heated to 1,000 °C in 1 h with Ar (500 sccm) followed by annealing in additional H_2 (5 sccm) for 40 min. Then CH_4 (1 sccm) was introduced as the carbon source for graphene growth for different durations. Finally, the system was cooled down naturally with Ar (1,000 sccm).

2.2 Mild-oxidation process

The as-grown graphene/Cu substrate was baked on a hot-plate heated to 150 °C. O_2/H_2O atmosphere was introduced by a humidifier. The humidity is about 5%–10%. The evolution of morphology of the baked graphene grain was monitored under an optical microscope.

2.3 H_2 etching and regrowth

After the CVD growth of graphene, the CH_4 was cut off and the sample was exposed to 5 sccm H_2 for 15 min at 1,000 °C to etch graphene, with flow of 500 sccm Ar. Then, CH_4 (1 sccm) was introduced into the system once again after H_2 etching to start the regrowth of graphene, under a 5 sccm H_2 and 500 sccm Ar.

2.4 Characterization

Optical images were taken with an Olympus microscope (Olympus BX51). Raman spectra were obtained with an alpha300R system (WITec, Germany) with a laser excitation wavelength of 633 nm and about 1 mW power. Scanning electron microscope (SEM) images and energy disperse spectroscopy (EDS) maps were obtained using a Thermal Fisher Quattro S Environmental SEM. The room temperature sheet resistance of graphene films was measured based on the four-point probe method to eliminate contact resistance. Each data is obtained from a 1 mm × 1 mm area.

3 Results and discussion

3.1 Eliminating the dot defects in graphene

In a common CVD graphene growth system, Cu foils are directly exposed to the atmosphere as substrates. During the high temperature growth, some small silica particles would be released and deposited on the Cu surface [26, 27] (Fig. 1(a) and Figs. S1(a) and S1(b) in the Electronic Supplementary Material (ESM)), which blocked the formation of completed graphene films (Fig. 1(c) and Fig. S2 in the ESM). Once this kind of graphene is used practically, the uniformity and quality of the film cannot be guaranteed, as the regions where the particles deposited exist a large amount of nanometre-scale dot defects, resulting in poor quality at these sites (upper panel of Figs. 1(e) and 1(f)).

Aiming at this issue, a specially designed heat-resisting box was introduced. The Cu foil was placed in the box and then loaded into the CVD system together. With this design, the released silica particles in the atmosphere are kept out of the box (Fig. 1(b)), and clean Cu surface can be obtained after annealing (Fig. S1(c) in the ESM). Then, high-quality graphene films without dot defects can be synthesized (Figs. 1(d)–1(f)). It is also worth noting that, for a traditional CVD graphene grown on Cu foil, the coverage of monolayer graphene is usually limited to 95%–98% [11]. This can be ascribed to silica particles which act as uncontrollable nucleation sites and induce bilayer

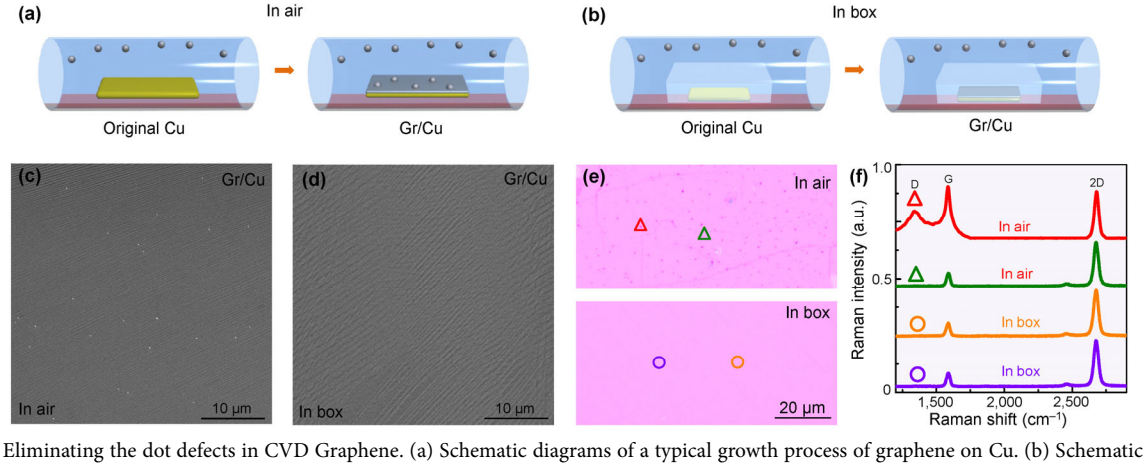

Figure 1 Eliminating the dot defects in CVD Graphene. (a) Schematic diagrams of a typical growth process of graphene on Cu. (b) Schematic diagrams of the heat-resisting box assisted growth process of graphene on Cu. (c) Representative SEM image of graphene produced without box. There are many particles on the surface. (d) Representative SEM image of graphene produced in a heat-resisting box. The surface is very clean and uniform. (e) Optical images of graphene transferred onto SiO_2/Si substrates without (upper panel) and with (lower panel) box. (f) Raman spectra of graphene obtained at position that marked in (e), obvious D band of graphene appears at the dot defect site marked with red triangle in (e).

or multilayer flakes (Fig. S2(a) in the ESM). By removing these nucleation sites in our experiment, almost complete monolayer graphene can be produced (Fig. S3 in the ESM).

3.2 Detecting point defects by a mild-oxidation technique

In addition to dot defects, point defects in CVD graphene are another issue that must be solved to realize the production of intrinsically pure graphene, where an effective defect detecting method with high throughput is the prerequisite. Unlike nanometre-scale dot defects which could be identified directly under SEM, atomic-scale point defects are difficult to detect due to the requirement of extreme spatial resolution [28]. Generally, intact graphene lattice possesses unprecedented impermeability to any molecule or atom, except for proton [29]. But at the defect sites, some small reactive molecules or ions could pass through graphene and react with the underlying substrate [30–34]. Thus, these defective sites can be amplified and identified.

In our experiment, we adopted an extremely mild method to detect the point defects in graphene without destroying its lattice, otherwise would induce extra defects. The as-grown graphene samples were placed in an atmosphere of oxygen and water (O_2/H_2O) vapour, and then baked at 150 °C. Under such a relatively mild condition, the O_2/H_2O will continuously pass through the point or line defects, and react with the underlying Cu substrate to form Cu_2O [35]. Due to the difference of mass density and refractive index between Cu_2O and Cu, the volume and colour contrast of these sites would change dramatically. As time goes on, the size of Cu_2O can easily reach several hundred nanometres (schematically shown in Fig. S4 in the ESM), which can be clearly identified with high-throughput under optical microscope (Fig. 2(a)).

With this design, grain boundaries and point defects in graphene can be easily visualized after baking for about 40 h (Figs. 2(b) and 2(c)). The Raman spectra collected at the black spot (orange circle marked in Fig. 2(c)) showed D band of graphene along with distinct characteristic peak of Cu_2O, indicating the existence of defective structure and the oxidation of underlying Cu here (Fig. 2(d)). A grain boundary can be regarded as a periodic distribution of point defects whose period increases quickly with the decrease of the twist angle [36]. In the limiting case, when the twist angle tends to infinitesimal, the grain boundary defects would evolve into a series of individual point defects. We tested our technique with various twist angles and found that the grain boundary can be clearly observed even when the twist angle is indistinguishable (Figs. 2(e) and 2(f)), indicating that our method would be effective to identify the periodic point defects. Only in the case of θ = 0° (Fig. 2(g), so-called seamless stitching, where no defective structure will be formed [22]), no grain boundary was observed after a long time of baking.

Based on the experimental data, we can conclude that the designed mild-oxidation-assisted detecting technique could be effective to visualize the grain boundaries and point defects. Naturally, one of the important concerns is that whether all the defects can be detected. If only part of the point defects can be detected, the measured purity of graphene will be not credible, which could be fatal for future practical applications.

To address this concern, we chose some individual graphene grains and analysed the time evolution of detected point defects in each grain during baking for about 300 h. As the time went on, the number of detected point defects first increased rapidly and then stabilized at a certain value (Fig. 3). This phenomenon actually further confirmed the validity of our method. Since point defects are inevitable during growth process, there must be a certain value of point defects existing in a graphene grain. If our technique is effective to detect the point defects meanwhile harmless to the lattice structure, the number of visualized point defects should stop increasing when reaching this value. And this is the key difference from previous grain boundary detecting techniques, where the treatment is usually so rude that would induce new defects and the number of point defects would increase all the time. Therefore, our analysis has proved that this mild-oxidation-assisted detecting technique can detect all the point defects in a graphene grain without introducing additional ones.

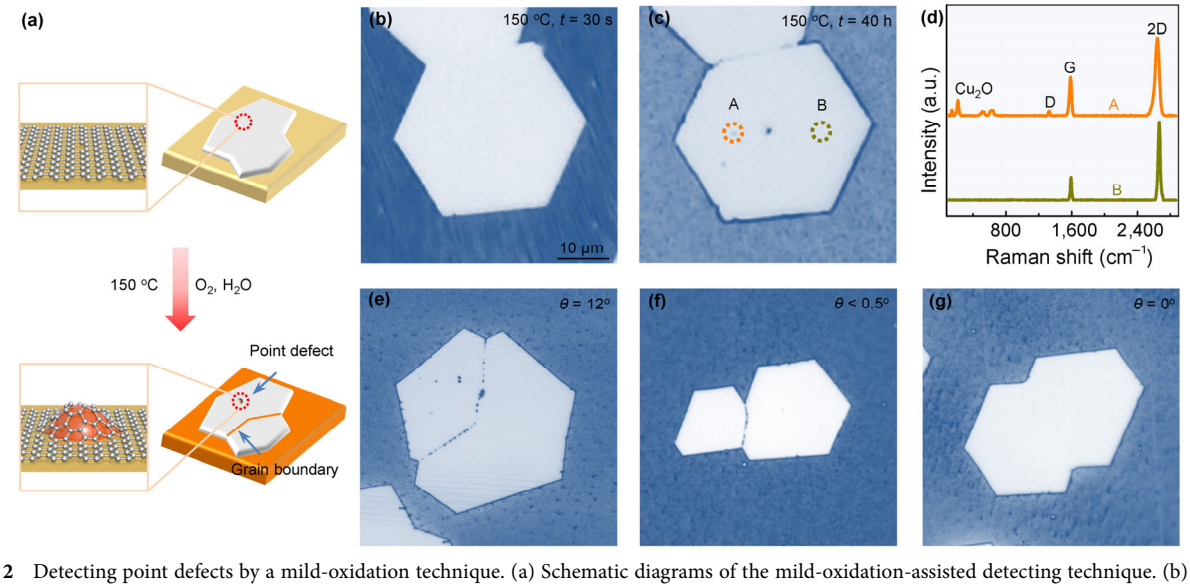

Figure 2 Detecting point defects by a mild-oxidation technique. (a) Schematic diagrams of the mild-oxidation-assisted detecting technique. (b) and (c) optical images of two merged graphene grains after baking at 150 °C for about 30 s (b) and 40 h (c), respectively. Grain boundary and the point defects can be visualized after the treatment. The image size of (b) and (c) is the same. (d) Raman spectra of graphene obtained at positons that marked in (c). At the position A, D band of graphene and characteristic peaks of Cu_2O appear, indicating the existence of defective structure and the oxidation of underlying Cu here. (e)–(g) Optical images of two merged graphene grains with the twist angles θ = 12° (e), θ < 0.5° (f), and θ = 0° (g) after baking for 40 h. The grain boundary can be clearly observed even when the twist angle is indistinguishable, indicating that our method is effective to identify the periodic point defects. The image size of (e)–(g) is same as (b).

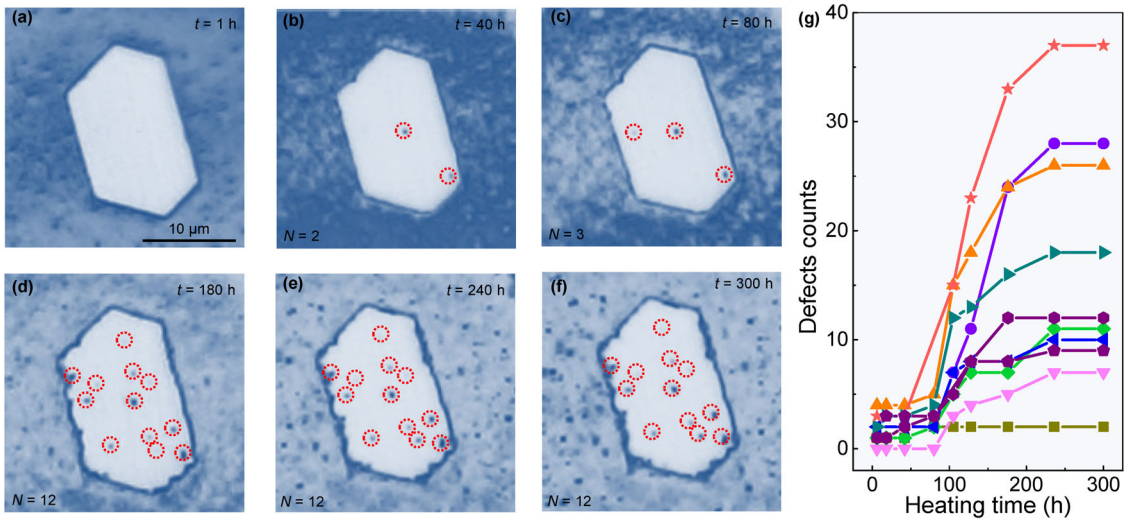

Figure 3 *In-situ* visualization of point defects in a graphene grain. (a)–(f) Time evolution optical images of a graphene grain during baking for about 300 h. As the time elapsed, the number of detected point defects first increased rapidly (a)–(d) and then stabilized at a certain value (d)–(f). The image size of (a)–(f) is the same. (g) Plot of the detected point defects in different graphene grain as a function of baking time. The value of detected point defects in all the grains we studied stopped at a certain value and would not increase anymore even after 300 h' baking.

3.3 Towards defect-free intrinsically pure graphene

Although the line and dot defects in graphene can be eliminated by single-crystal epitaxy growth and heat-resisting box, the point defects are inevitable during growth due to thermodynamic fluctuation. Fortunately, given by the two-dimensionality, the point defects in graphene are all on the surface, and thus can be cured by an extra etching-regrowth approach. It has been widely studied that the unstable defective sites (point defects, boundaries) will preferentially react with hydrogen (H_2) and form etched holes [37]. Once the dot defects are eliminated (only point defects left), the holes can be cured during the regrowth process, and an intact graphene monolayer can be obtained (Fig. 4(a)). However, in traditional CVD method, dot defects with particles existed on the surface, so graphene would always be incomplete, no matter how many times etching and regrowth processes (Fig. 4(b)).

With the introduction of a heat-resisting box, ultrahigh-quality graphene can be obtained after etching and regrowth of the dot-defect-free graphene samples. The purity of synthesized graphene was firstly checked by the mild-oxidation process and no point defect (or only the central nucleation site) can be visualized (Fig. 4(c) and Fig. S5(a) in the ESM), indicating the point defect density < 1/1,000 μm^2. After H_2 etching, no holes appeared in the grain (or the nucleation centre was etched and formed only one hole, Fig. 4(d) and Fig. S5(b) in the ESM). The shape of the graphene grains was transformed from sharp hexagon to rounded hexagon as the etching could only happen at the edges. As a contrast, the sample with dot defects still shows lots of black spots after mild oxidation and etched holes in the grain after H_2 etching, even after etching and regrowth process (Figs. 4(e) and 4(f)).

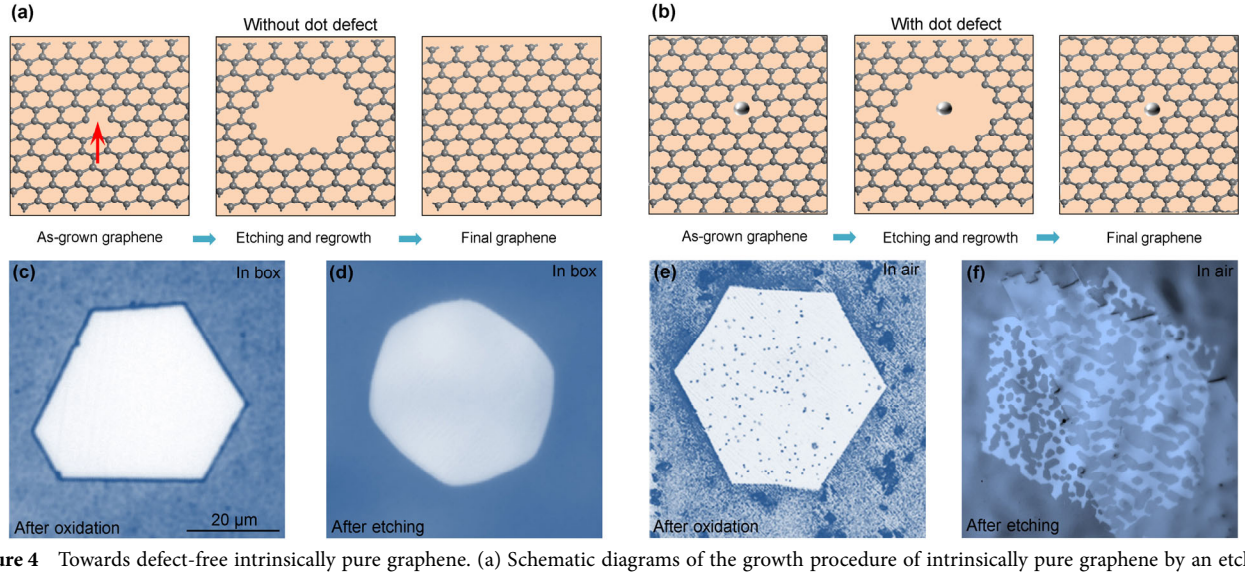

Figure 4 Towards defect-free intrinsically pure graphene. (a) Schematic diagrams of the growth procedure of intrinsically pure graphene by an etching and regrowth method. The point defect can be etched and then cured during the process, and thus an intact graphene monolayer can be obtained. (b) Schematic diagrams of the graphene growth process with dot defects by the etching and regrowth method. As dot defects with particles existing on the surface, graphene will always be incomplete. (c) Optical image of an intrinsically pure graphene grain after mild oxidation. No point defect can be visualized. (d) Optical image of an intrinsically pure graphene grain after H_2 etching. No holes appeared in the grain and the shape was transformed from sharp hexagon to rounded hexagon as the etching could only happen at the edges. (e) and (f) Optical images of graphene grains with dot defects after oxidation (e) and H_2 etching (f). As particles existing on the surface, these dot defects cannot be removed by the etching and regrowth method. The image size of (c)–(f) is the same.

The technique was also applicable to continuous graphene films (Fig. S6 in the ESM) and the quality was tested by sheet resistance measurements. By eliminating the dot and point defects, sheet resistances of graphene films were greatly decreased (Fig. S7 in the ESM).

4 Conclusions

In conclusion, we proposed an approach to realize the production of intrinsically pure monolayer graphene grown on Cu by eliminating both the dot and point defects in grains. Combining the heat-resisting box and etching-regrowth technique, ultrahigh pure graphene with point defects density < 1/1,000 μm^2 has been successfully produced. Our finding points out an avenue for the synthesis of intrinsically pure graphene and lays foundation for the high-end applications of graphene at the integrated-circuit level.

Acknowledgements

This work was supported by The Key R&D Program of Guangdong Province (Nos. 2019B010931001, 2020B010189001, and 2018B030327001), Guangdong Provincial Science Fund for Distinguished Young Scholars (No. 2020B1515020043), Science and Technology Program of Guangzhou (No. 2019050001), Beijing Natural Science Foundation (No. JQ19004), the National Natural Science Foundation of China (Nos. 52025023, 51991340, and 51991342), National Key R&D Program of China (Nos. 2016YFA0300903 and 2016YFA0300804), Beijing Excellent Talents Training Support (No. 2017000026833ZK11), Beijing Municipal Science & Technology Commission (No. Z191100007219005), Beijing Graphene Innovation Program (No. Z181100004818003), The Strategic Priority Research Program of Chinese Academy of Sciences (No. XDB33000000), Bureau of Industry and Information Technology of Shenzhen (Graphene platform No. 201901161512), Guangdong Innovative and Entrepreneurial Research Team Program (No. 2016ZT06D348), the Science, Technology, Innovation Commission of Shenzhen Municipality (No. KYTDPT20181011104202253), The Pearl River Talent Recruitment Program of Guangdong Province (No. 2019ZT08C321), and China Postdoctoral Science Foundation (Nos. 2019M660280, 2019M660281, and 2020T130022).

Electronic Supplementary Material: Supplementary material (EDS measurements, SEM of Cu foils before and after annealing and optical images of continuous graphene films) is available in the online version of this article at http://doi.org/10.1007/s12274-021-3575-9.

References

[1] Duan, X. F.; Huang, Y.; Cui, Y.; Wang, J. F.; Lieber, C. M. Indium phosphide nanowires as building blocks for nanoscale electronic and optoelectronic devices. *Nature* **2001**, *409*, 66–69.

[2] Johnson, J. C.; Choi, H. J.; Knutsen, K. P.; Schaller, R. D.; Yang, P. D.; Saykally, R. J. Single gallium nitride nanowire lasers. *Nat. Mater.* **2002**, *1*, 106–110.

[3] Madar, R. Materials science: Silicon carbide in contention. *Nature* **2004**, *430*, 974–975.

[4] Nakamura, D.; Gunjishima, I.; Yamaguchi, S.; Ito, T.; Okamoto, A.; Kondo, H.; Onda, S.; Takatori, K. Ultrahigh-quality silicon carbide single crystals. *Nature* **2004**, *430*, 1009–1012.

[5] Geim, A. K.; Novoselov, K. S. The rise of graphene. *Nat. Mater.* **2007**, *6*, 183–191.

[6] Castro Neto, A. H.; Guinea, F.; Peres, N. M. R.; Novoselov, K. S.; Geim, A. K. The electronic properties of graphene. *Rev. Mod. Phys.* **2009**, *81*, 109–162.

[7] Bonaccorso, F.; Sun, Z.; Hasan, T.; Ferrari, A. C. Graphene photonics and optoelectronics. *Nat. Photonics* **2010**, *4*, 611–622.

[8] Novoselov, K. S.; Fal'ko, V. I.; Colombo, L.; Gellert, P. R.; Schwab, M. G.; Kim, K. A roadmap for graphene. *Nature* **2012**, *490*, 192–200.

[9] Fiori, G.; Bonaccorso, F.; Iannaccone, G.; Palacios, T.; Neumaier, D.; Seabaugh, A.; Banerjee, S. K.; Colombo, L. Electronics based on two-dimensional materials. *Nat. Nanotechnol.* **2014**, *9*, 768–779.

[10] Sutter, P. W.; Flege, J. I.; Sutter, E. A. Epitaxial graphene on ruthenium. *Nat. Mater.* **2008**, *7*, 406–411.

[11] Li, X. S.; Cai, W. W.; An, J. H.; Kim, S.; Nah, J.; Yang, D. X.; Piner, R.; Velamakanni, A.; Jung, I.; Tutuc, E. et al. Large-area synthesis of high-quality and uniform graphene films on copper foils. *Science* **2009**, *324*, 1312–1314.

[12] Reina, A.; Jia, X. T.; Ho, J.; Nezich, D.; Son, H.; Bulovic, V.; Dresselhaus, M. S.; Kong, J. Large area, few-layer graphene films on arbitrary substrates by chemical vapor deposition. *Nano Lett.* **2009**, *9*, 30–35.

[13] Bae, S.; Kim, H.; Lee, Y.; Xu, X. F.; Park, J. S.; Zheng, Y.; Balakrishnan, J.; Lei, T.; Kim, H. R.; Song, Y. I. et al. Roll-to-roll production of 30-inch graphene films for transparent electrodes. *Nat. Nanotechnol.* **2010**, *5*, 574–578.

[14] Geng, D. C.; Wu, B.; Guo, Y. L.; Huang, L. P.; Xue, Y. Z.; Chen, J. Y.; Yu, G.; Jiang, L.; Hu, W. P.; Liu, Y. Q. Uniform hexagonal graphene flakes and films grown on liquid copper surface. *Proc. Natl. Acad. Sci. USA* **2012**, *109*, 7992–7996.

[15] Gao, L. B.; Ren, W. C.; Xu, H. L.; Jin, L.; Wang, Z. X.; Ma, T.; Ma, L. P.; Zhang, Z. Y.; Fu, Q.; Peng, L. M. et al. Repeated growth and bubbling transfer of graphene with millimetre-size single-crystal grains using platinum. *Nat. Commun.* **2012**, *3*, 699.

[16] Yan, Z.; Lin, J.; Peng, Z. W.; Sun, Z. Z.; Zhu, Y.; Li, L.; Xiang, C. S.; Samuel, E. L.; Kittrell, C.; Tour, J. M. Toward the synthesis of wafer-scale single-crystal graphene on copper foils. *ACS Nano* **2012**, *6*, 9110–9117.

[17] Hao, Y. F.; Bharathi, M. S.; Wang, L.; Liu, Y. Y.; Chen, H.; Nie, S.; Wang, X. H.; Chou, H.; Tan, C.; Fallahazad, B. et al. The role of surface oxygen in the growth of large single-crystal graphene on copper. *Science* **2013**, *342*, 720–723.

[18] Zhou, H. L.; Yu, W. J.; Liu, L. X.; Cheng, R.; Chen, Y.; Huang, X. Q.; Liu, Y.; Wang, Y.; Huang, Y.; Duan, X. F. Chemical vapour deposition growth of large single crystals of monolayer and bilayer graphene. *Nat. Commun.* **2013**, *4*, 2096.

[19] Gao, L. B.; Ni, G. X.; Liu, Y. P.; Liu, B.; Neto, A. H. C.; Loh, K. P. Face-to-face transfer of wafer-scale graphene films. *Nature* **2014**, *505*, 190–194.

[20] Lee, J. H.; Lee, E. K.; Joo, W. J.; Jang, Y.; Kim, B. S.; Lim, J. Y.; Choi, S. H.; Ahn, S. J.; Ahn, J. R.; Park, M. H. et al. Wafer-scale growth of single-crystal monolayer graphene on reusable hydrogen-terminated germanium. *Science* **2014**, *344*, 286–289.

[21] Babenko, V.; Murdock, A. T.; Koós, A. A.; Britton, J.; Crossley, A.; Holdway, P.; Moffat, J.; Huang, J.; Alexander-Webber, J. A.; Nicholas, R. J. et al. Rapid epitaxy-free graphene synthesis on silicidated polycrystalline platinum. *Nat. Commun.* **2015**, *6*, 7536.

[22] Nguyen, V. L.; Shin, B. G.; Duong, D. L.; Kim, S. T.; Perello, D.; Lim, Y. J.; Yuan, Q. H.; Ding, F.; Jeong, H. Y.; Shin, H. S. et al. Seamless stitching of graphene domains on polished copper (111) foil. *Adv. Mater.* **2015**, *27*, 1376–1382.

[23] Wu, T. R.; Zhang, X. F.; Yuan, Q. H.; Xue, J. C.; Lu, G. Y.; Liu, Z. H.; Wang, H. S.; Wang, H. M.; Ding, F.; Yu, Q. K. et al. Fast growth of inch-sized single-crystalline graphene from a controlled single nucleus on Cu–Ni alloys. *Nat. Mater.* **2016**, *15*, 43–47.

[24] Xu, X. Z.; Zhang, Z. H.; Dong, J. C.; Yi, D. C.; Niu, J. J.; Wu, M. H.; Lin, L.; Yin, R. K.; Li, M. Q.; Zhou, J. Y. et al. Ultrafast epitaxial growth of metre-sized single-crystal graphene on industrial cu foil. *Sci. Bull.* **2017**, *62*, 1074–1080.

[25] Vlassiouk, I. V.; Stehle, Y.; Pudasaini, P. R.; Unocic, R. R.; Rack, P. D.; Baddorf, A. P.; Ivanov, I. N.; Lavrik, N. V.; List, F.; Gupta, N. et al. Evolutionary selection growth of two-dimensional materials on polycrystalline substrates. *Nat. Mater.* **2018**, *17*, 318–322.

[26] Yasunishi, T.; Takabayashi, Y.; Kishimoto, S.; Kitaura, R.; Shinohara, H.; Ohno, Y. Origin of residual particles on transferred graphene grown by CVD. *Jpn. J. Appl. Phys.* **2016**, *55*, 080305.

[27] Lisi, N.; Dikonimos, T.; Buonocore, F.; Pittori, M.; Mazzaro, R.; Rizzoli, R.; Marras, S.; Capasso, A. Contamination-free graphene by chemical vapor deposition in quartz furnaces. *Sci*. *Rep*. **2017**, *7*, 9927.

[28] Huang, P. Y.; Ruiz-Vargas, C. S.; van der Zande, A. M.; Whitney, W. S.; Levendorf, M. P.; Kevek, J. W.; Garg, S.; Alden, J. S.; Hustedt, C. J.; Zhu, Y. et al. Grains and grain boundaries in single-layer graphene atomic patchwork quilts. *Nature* **2011**, *469*, 389–392.

[29] Hu, S.; Lozada-Hidalgo, M.; Wang, F. C.; Mishchenko, A.; Schedin, F.; Nair, R. R.; Hill, E. W.; Boukhvalov, D. W.; Katsnelson, M. I.; Dryfe, R. A. W. et al. Proton transport through one-atom-thick crystals. *Nature* **2014**, *516*, 227–230.

[30] Duong, D. L.; Han, G. H.; Lee, S. M.; Gunes, F.; Kim, E. S.; Kim, S. T.; Kim, H.; Ta, Q. H.; So, K. P.; Yoon, S. J. et al. Probing graphene grain boundaries with optical microscopy. *Nature* **2012**, *490*, 235–239.

[31] Kim, D. W.; Kim, Y. H.; Jeong, H. S.; Jung, H. T. Direct visualization of large-area graphene domains and boundaries by optical birefringency. *Nat*. *Nanotechnol*. **2012**, *7*, 29–34.

[32] Son, J. H.; Baeck, S. J.; Park, M. H.; Lee, J. B.; Yang, C. W.; Song, J. K.; Zin, W. C.; Ahn, J. H. Detection of graphene domains and defects using liquid crystals. *Nat*. *Commun*. **2014**, *5*, 3484.

[33] Ago, H.; Fukamachi, S.; Endo, H.; Solis-Fernández, P.; Yunus, R. M.; Uchida, Y.; Panchal, V.; Kazakova, O.; Tsuji, M. Visualization of grain structure and boundaries of polycrystalline graphene and two-dimensional materials by epitaxial growth of transition metal dichalcogenides. *ACS Nano* **2016**, *10*, 3233–3240.

[34] Fan, X. G.; Wagner, S.; Schädlich, P.; Speck, F.; Kataria, S.; Haraldsson, T.; Seyller, T.; Lemme, M. C.; Niklaus, F. Direct observation of grain boundaries in graphene through vapor hydrofluoric acid (VHF) exposure. *Sci*. *Adv*. **2018**, *4*, eaar5170.

[35] Xu, X. Z.; Yi, D.; Wang, Z. C.; Yu, J. C.; Zhang, Z. H.; Qiao, R. X.; Sun, Z. H.; Hu, Z. H.; Gao, P.; Peng, H. L. et al. Greatly enhanced anticorrosion of Cu by commensurate graphene coating. *Adv*. *Mater*. **2018**, *30*, 1702944.

[36] Yazyev, O. V.; Louie, S. G. Electronic transport in polycrystalline graphene. *Nat*. *Mater*. **2010**, *9*, 806–809.

[37] Zhang, Y.; Li, Z.; Kim, P.; Zhang, L. Y.; Zhou, C. W. Anisotropic hydrogen etching of chemical vapor deposited graphene. *ACS Nano* **2012**, *6*, 126–132.